



Novel approach for the utilization of ionic liquid-based cellulose derivative biosourced polymer electrolytes in safe sodium-ion batteries

Mohd Saiful Asmal Rani^{1,3} · Masita Mohammad¹ · Mohd Sukor Sua'it¹ · Azizan Ahmad² · Nor Sabirin Mohamed³

Received: 14 June 2020 / Revised: 16 August 2020 / Accepted: 23 September 2020 /
Published online: 1 October 2020
© Springer-Verlag GmbH Germany, part of Springer Nature 2020

Abstract

Carboxymethyl cellulose (CMC) derived from kenaf bast fiber complexed with sodium acetate and integrated with ionic liquid 1-butyl-3-methylimidazolium chloride, [Bmim]Cl, was investigated as potential biosourced polymer electrolyte. The highest ionic conductivity of $(4.54 \pm 1.2) \times 10^{-3} \text{ S cm}^{-1}$ was obtained after introducing 30 wt% [Bmim]Cl with respect to the weight of CMC. Infrared spectroscopic analysis revealed the interaction of the polymer host with the sodium salt and ionic liquid. Ion transport analysis showed that charge transport in the biopolymer electrolyte system occurred predominately with ion and sodium ion transference numbers of 0.129. Linear sweep voltammetry result showed that electrochemical stability reached $\sim 2.9 \text{ V}$, showing that the biopolymer electrolyte is suitable for practical application in electrochemical devices. Sodium battery configurations of Na/CH₃COONa-30 wt% [Bmim]Cl/I₂+C+electrolyte were fabricated and demonstrated an initial discharge capacity of 1.5 mAh for 200 h with 1.6 V open circuit potential.

Keywords Battery · Biosources · Cellulose · Electrochemical · Energy storage

Introduction

Over the past decades, energy storage has become a global concern as a result of skyrocketing energy demands and the growing understanding of the environmental consequences of using fossil fuels. A strong call for alternative energy sources has been initiated worldwide to address these problems. The increasing use of renewable

✉ Mohd Saiful Asmal Rani
iker.asmal55@gmail.com

✉ Masita Mohammad
masita@ukm.edu.my

Extended author information available on the last page of the article

energy sources (wind, solar, etc.) is facing several crucial challenges including modulating variable renewable resources from time to time, integrating them into the grid smoothly and balancing electricity generation and demand in peak and off-peak periods [1–4]. The exploration of energy storage technologies especially battery technology for large-scale storage is essential and could be a solution to these global concerns [5].

The most common type of rechargeable batteries found in almost all portable electronic devices is the lithium-ion battery (LIB). Li-based electrochemistry has several merits such as small ionic radius size (allows rapid diffusion in solids), low redox potential versus the standard hydrogen electrode, and facilitation of high cell voltage, high energy density and low weight (enables the use of high-specific energy devices) [6–10]. Aside from these properties, LIBs have a long cycle life and rate capability, making this technology dominate the portable electronics market. Although LIBs remain to be an important energy storage technology, many concerns such as massive consumption of limited Li resource high cost and long-term availability have arisen. Increasing Li utilization in medium-scale automotive batteries will ultimately increase the price of Li compounds, thereby making large-scale storage prohibitively expensive. Moreover, current lithium battery technology has limitations such as unstable metal electrolyte interfaces, volatile and potentially flammable electrolytes [11–13].

As a potential solution to overcome the issues related to LIBs, the use of Na in batteries could economically mitigate the shortage of Li due to the high abundance and broad distribution of Na sources [14]. Given that Na is located just below Li in the s orbital, similar chemical approaches, such as synthetic strategies, intercalation, conversion chemistry and characterization methods that are utilized in materials for LIBs could be applied to investigate materials for Na-ion batteries (NIBs) efficiently [15, 16]. The large size and different bonding characteristics of Na ions influence the thermodynamic/kinetic properties of NIBs, leading to unexpected behaviors in electrochemical performance and reaction mechanism in comparison with LIBs. Moreover, Na (when used as secondary batteries) is inexpensive and has a low toxicity, low atomic mass and a suitable redox potential; hence, NIBs have great potential for energy storage applications [17–19]. Focusing on the NIB topic, Bella et al. [20] attempted to synthesize poly(glycidyl ether)s from industrial byproducts doped with sodium bis(fluorosulfonyl)imide, and obtained conductivity exceeding 10^{-5} S cm⁻¹ and a reasonably wide electrochemical stability. Chen et al. [21] developed NIBs by using a flexible PPEGMA-based gel polymer electrolyte (PGT32-5%) plasticized by non-flammable triethyl phosphate and supported by glass fiber. The highest conductivity of 9.1×10^{-4} S cm⁻¹ was obtained at 27 °C and a wide electrochemical window (4.8 V).

The present work aims to develop a new type of Na ion conducting biopolymer electrolyte (BPE) integrated with ionic liquid acting as a plasticizer and carboxymethyl cellulose (CMC) derived from kenaf bast fiber serving as the polymer host. Limited work has been conducted on the use of biopolymer-ionic liquid to develop NIBs. With this situation as motivation, this study attempted to produce CMC-CH₃COONa-Bmim[Cl] biopolymer electrolytes. The resultant electrolyte films were characterized through Fourier transform infrared analysis (FTIR), scanning electron

microscopy (SEM), thermogravimetric analysis (TGA), electrochemical impedance spectroscopy (EIS), chronoamperometry (t_{ion} and t_{Na}^+) and linear sweep voltammetry (LSV).

Experimental

Materials

Kenaf Fiber Industry Sdn. Bhd. (Malaysia) provided raw kenaf bast fibers as the main material to be isolated to cellulose and subsequently to CMC via chemical modification in accordance with previous work [22]. Sodium hydroxide (99%), isopropanol (98%), sulfuric acid (98%), glacial acetic acid (99.5%), monochloroacetic acid and sodium chlorite (80%) were purchased from Sigma-Aldrich and System-chemAR. These chemicals were used without additional purification.

Preparation of electrolytes

Chemically purified cellulose from kenaf bast fiber was isolated in accordance with a previous study [22]. The cellulose was modified into CMC, and its degree of substitution value was 1.49. Conventional solution casting was conducted to form thick electrolyte films with a concentration variation of CH_3COONa (10, 20, 30 and 40 wt%). The solid components were dissolved in 40 ml of 1% acetic acid at room temperature. Complete dissolution was obtained after a few hours of stirring at ambient temperature by using a magnetic stirrer. The homogeneous solution was then transferred into glass Petri dishes and left to dry to form thin films. All films were relocated to desiccator for further drying.

Electrolytes characterization

Chemical interactions were investigated using a Perkin Elmer Frontier (FTIR) spectrometer equipped with attenuated total reflection (ATR). The sample was placed on the top of a diamond surface. A pressure arm applied force on the sample, and infrared light passed through the sample. FTIR spectra were recorded in the spectral range of $4000\text{--}550\text{ cm}^{-1}$ ($\pm 1.0\text{ cm}^{-1}$) at a scan resolution of 2 cm^{-1} at room temperature. The FTIR data were recorded in transmittance mode. The surface morphology of each biopolymer electrolyte (BPE) film was observed using a Zeiss EVO MA10 scanning electron microscope at $500\times$, $1000\times$ and $2000\times$ magnification (minimum instrumentation resolution of $\sim 100\text{ nm}$) with a 10 kV electron beam. BPE samples were sputter-coated with gold by coating a machine for 90 s before analysis to prevent charging. Thermal analysis of BPE films was conducted from ambient temperature to up to $600\text{ }^\circ\text{C}$ ($\pm 1.0\text{ }^\circ\text{C}$ instrument accuracy) at a heating rate of $10\text{ }^\circ\text{C min}^{-1}$ by using a Setaram EVO Labsys thermal analyzer in nitrogen atmosphere. The data were then analyzed with Calisto software. Impedance measurement of the films was performed with a Solartron 1260 impedance/gain phase analyzer at

a frequency range of 10 Hz to 4 MHz ($\pm 1.0\%$ accuracy). Impedance spectroscopy was used to determine the ionic conductivity of the BPE films at a temperature range from 30 to 65 °C. The films were cut into a suitable size and sandwiched between two stainless steel electrodes with a diameter of 2 cm under spring pressure; the electrodes were connected to a computer [23]. Ionic transference number measurement was conducted using a direct current polarization technique by monitoring the polarization current as a function of time. The current decayed gradually with time and approached the steady state (saturated). The biopolymer electrolyte films were sandwiched between two stainless steel blocking electrodes connected to a voltage source (1.0 V) by using Wagner's polarization technique [24]. Na transference number measurement has also been conducted in a previous work by sandwiching a BPE between Na metal layers on the top of a steel blocking electrode connected to a voltage source [25]. Solid-state electrochemical cells were fabricated with a configuration of Na/CMC-CH₃COONa-30 wt% [Bmim]Cl/I₂ + C + electrolyte. The discharge characteristics of the cells were monitored under a constant current of 0.1 mA and tested using a NEWARE BTS 3000 battery tester interfaced with a computer. Experimental and measurement errors were calculated based on the standard deviation of a minimum of three independent samples measured.

Results and discussion

Fourier transform infrared spectroscopy

FTIR spectroscopy was performed on the CMC-CH₃COONa-[Bmim]Cl biopolymer electrolyte films to explore the interactions among the host polymer, ionic salt and ionic liquid. The FTIR spectra of pure CMC, CMC-30 wt% CH₃COONa and CMC-CH₃COONa containing 30 wt% [Bmim]Cl in the 4000–550 cm⁻¹ spectral range are shown in Fig. 1. Figure 1c shows the effects of CH₃COONa salt on the CMC FTIR spectrum. The stretching mode of COO⁻ in the carboxylic group attributed as the main backbone of CMC was detected at 1552 cm⁻¹ [26, 27].

The symmetry of the C=O stretching band of CMC shifted from 1597 to 1548 cm⁻¹ after the addition of CH₃COONa to the CMC-salt system. This result suggests that the cation (Na⁺) substructure in CH₃COONa interacted with (C=O) in pure CMC. Characteristic C–O stretching on the polysaccharide skeleton [28, 29] was observed at 1040 cm⁻¹. The minor shifting of the band at 1057 cm⁻¹ to low wavenumbers proves that complexation had occurred. The bands observed at 1411 and 1325 cm⁻¹ were due to the stretching mode of –CH₂ scissoring and the –OH bending vibration of CMC, respectively [30].

The introduction of 30 wt% [Bmim]Cl to the biopolymer electrolyte system shifted the asymmetric stretching of COO⁻ in CMC-CH₃COONa at 1552 cm⁻¹ to a high wavenumber (1565 cm⁻¹). Samsudin and co-researchers [31] reported a similar effect in their study where the asymmetric stretching peak of COO⁻ in carboxymethyl carrageenan shifted to a high wavenumber upon the inclusion of an ionic liquid. This result reveals that [Bmim]Cl was successfully integrated into the biopolymer electrolyte complexes. The incorporation of [Bmim]Cl theoretically weakened

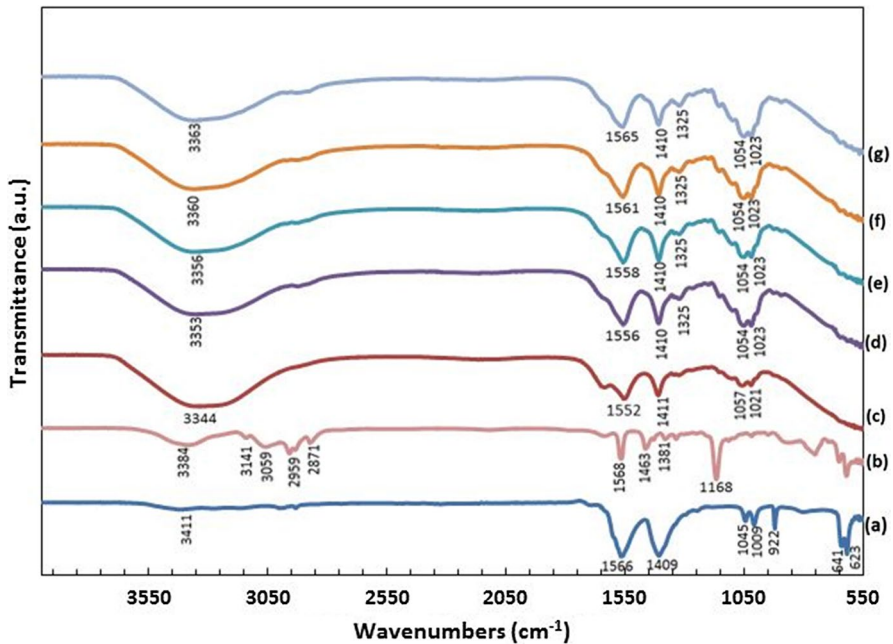


Fig. 1 FTIR spectra of **a** sodium acetate salt, **b** [Bmim]Cl, **c** CMC-CH₃COONa, **d** CMC-CH₃COONa-10 wt% [Bmim]Cl, **e** CMC-CH₃COONa-20 wt% [Bmim]Cl, **f** CMC-CH₃COONa-30 wt% [Bmim]Cl and **g** CMC-CH₃COONa-40 wt% [Bmim]Cl

the dipole–dipole interactions in the polymer chains, thus reducing the solvation of Na⁺ by the polymer matrix and enhancing the segmental motion of the biopolymer electrolytes.

Surface morphology

Figure 2 illustrates the surface morphology of the pure CMC, CMC-CH₃COONa and CMC-CH₃COONa-30 wt% [Bmim]Cl films at 1000× magnification. As shown in Fig. 2a, pure CMC had a rough and uneven surface, and a few cubic shapes of various sizes were visible in a certain area. When CH₃COONa was complexed with CMC, the film acquired a smoother morphology than that before, as shown in Fig. 2b. With the addition of [Bmim]Cl, the film surface was further smoothed as illustrated in Fig. 2c, indicating that the sample was highly amorphous. This result might be due to the plasticizing effect of [Bmim]Cl, which acted as a plasticizer in the polymer host.

Thermal properties

Figure 3 shows TGA curves of CMC-CH₃COONa comprising 0, 10, 20, 30 and 40 wt% of [Bmim]Cl biopolymer electrolytes. As can be observed from the TGA

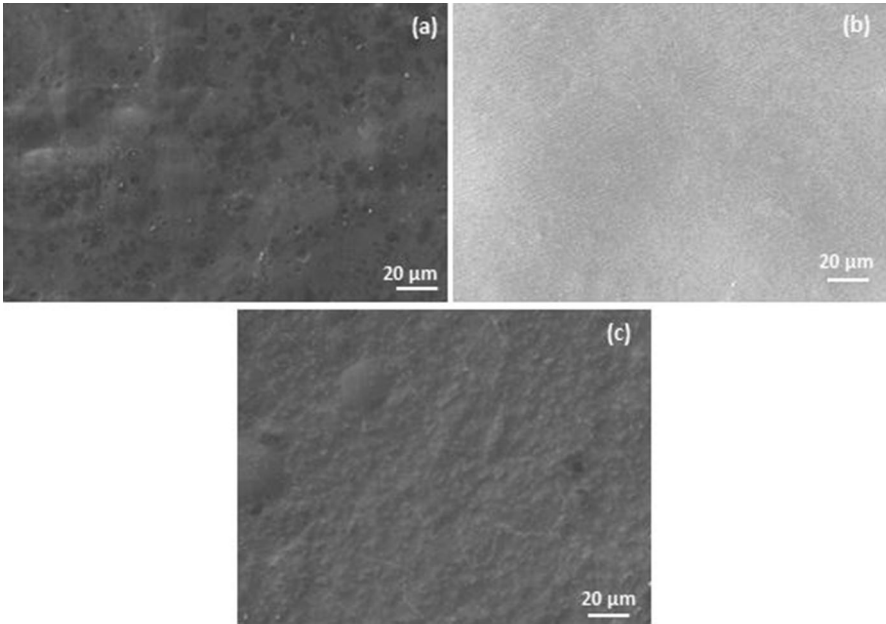


Fig. 2 Surface morphology of **a** pure CMC, **b** CMC-CH₃COONa and **c** CMC-CH₃COONa-30 wt% [Bmim]Cl films

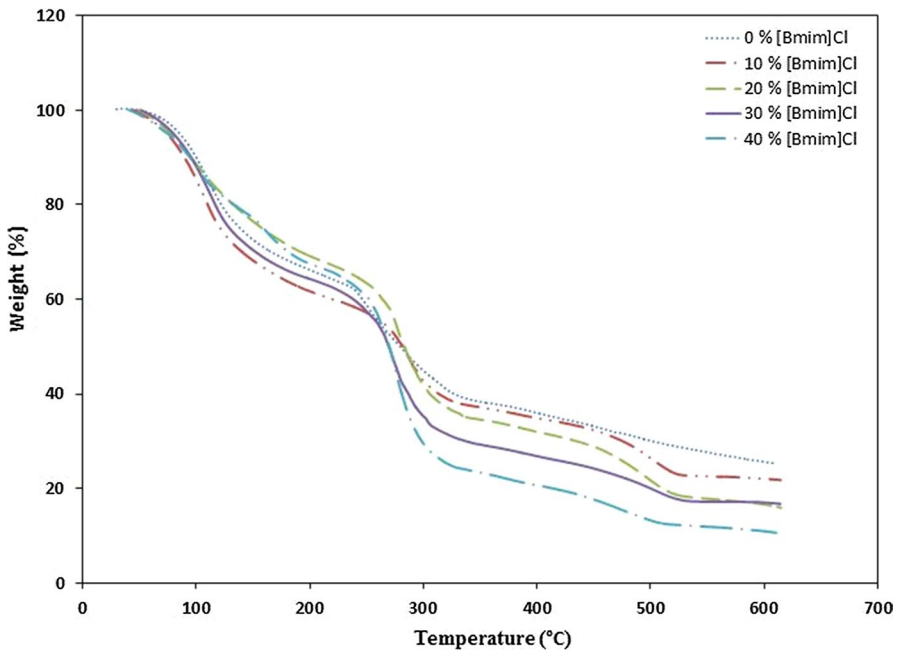


Fig. 3 TGA curves of CMC-CH₃COONa containing **a** 0 wt%, **b** 10 wt%, **c** 20 wt%, **d** 30 wt% and **e** 40 wt% of [Bmim]Cl

curves, two distinct stages occurred. Initial loss occurred around 16.57–18.2% (at a temperature range of 30 to 120 °C) in all BPE films, which can be explained by the existence of entrapped moisture in the films [32]. Edmond and co-workers [33] also obtained comparable observations in their study. This result can be explained by the capability of the biopolymer to capture moisture from its environment throughout the evaporation of solvents in the BPE films [34]. The second loss was attributed to the decarboxylation of CMC.

The incorporation of [Bmim]Cl into the CMC-CH₃COONa system produced an enhancement in thermal stability and heat resistivity, confirming that the ionic liquids in the polymer electrolytes played an important role in enhancing the thermal properties [35]. Upon the addition of [Bmim]Cl, the decomposition temperature T_d increased. However, the total weight of the BPE film decreased. Figure 3 indicates that the BPE samples doped with 30 wt% of [Bmim]Cl exhibited the highest T_d at a temperature of 307.5 °C with a total weight loss of 66.8%. This phenomenon can be explained by the loss of COO⁻ from the CMC backbone [36], which interacted with CH₃COONa and [Bmim]Cl as discussed in FTIR results. However, T_d increased linearly upon the incorporation of [Bmim]Cl which may be explained by the complexation that occurred and required a high temperature to disrupt the bonding [37]. Moreover, the existence of an amorphous region in the BPE film enhanced the heat sensitivity. Given the thermal stability, only a small amount of the monomer was detached from the complex structure of the BPE, thus reducing the total weight loss.

Analysis of electrochemical properties

Complex impedance spectroscopy analysis

The Nyquist plot of the BPE film of the CMC, 30 wt% CH₃COONa, 30 wt% [Bmim]Cl system at various temperatures is displayed in Fig. 4. No semicircle is found in the plot, indicating the dominance of the resistive and constant phase element of the polymer electrolyte system [38]. The Nyquist spectra showed a low-frequency spike, suggesting that ions were the main contributor to conduction. A comparable observation was acquired by Jacob et al. [39]. Spikes at an angle of less than 90° to the real axis were achieved in this study because of the diffusion on the rough electrode electrolyte interfaces [40]. Conductivity was calculated using:

$$\sigma = \frac{t}{R_b A} \quad (1)$$

where t is the sample thickness, R_b is the bulk resistance, and A is the surface area.

The Nyquist plot of the CMC-CH₃COONa impregnated with 30 wt% [Bmim]Cl film BPE at various temperatures is depicted in Fig. 4. Conductivity increased to an optimized value of 30 wt% [Bmim]Cl and settled at 40 wt% [Bmim]Cl. The pristine CMC conductivity was $(7.51 \pm 1.4) \times 10^{-5}$ S cm⁻¹, and CMC-30 wt% CH₃COONa possessed a conductivity value of $(2.83 \pm 1.1) \times 10^{-3}$ S cm⁻¹. The conductivity enhanced to $(2.92 \pm 1.2) \times 10^{-3}$ S cm⁻¹ upon the incorporation of 10 wt% of [Bmim]Cl. The highest conductivity value of $(4.54 \pm 1.2) \times 10^{-3}$ S cm⁻¹ was achieved with

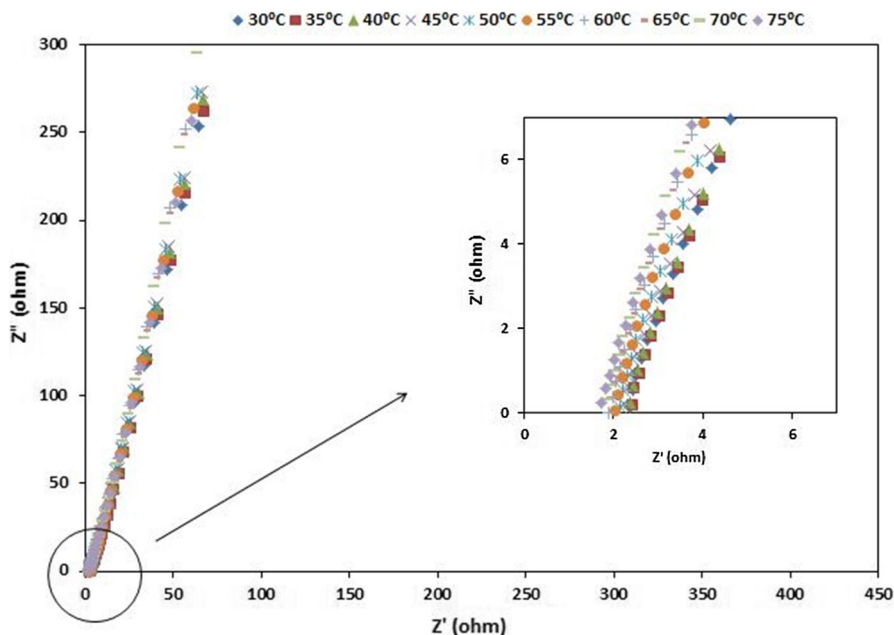


Fig. 4 Nyquist plot for CMC-CH₃COONa impregnated with 30 wt% [Bmim]Cl film at various temperatures

30 wt% loading of [Bmim]Cl. The increasing trend of conductivity with [Bmim]Cl addition can be explained by the ion mobility addition in the polymer electrolyte system. This phenomenon is the result of the [Bmim]Cl plasticizing effect. This effect weakens dipole–dipole interactions in the polymer chains, thus reducing the solvation of Na⁺ by the polymer matrix. Hence, it promotes ionic decoupling, enhances the dynamic free volume of the polymer system and improves the ionic conductivity [41]. According to Anuar et al. [42], an ionic liquid weakens polymer–polymer chain interactions and decreases dipole–ion interactions in dopant salt. Moreover, the plasticizing effect lowers T_g , softens the polymer backbone and increases the segmental mobility when an electric field is applied across the biopolymer electrolyte, leading to an increase in ionic conductivity [43] (Fig. 5).

However, after the incorporation of 40 wt% [Bmim]Cl, the ionic conductivity decreased drastically possibly due to the formation of neutral ion/non-conducting ion aggregates that reduce the number of mobile ions and cause the biopolymer electrolytes to become increasingly dense [44]. In addition, the decrease may have been caused by the creation of ion aggregates or ion multiples which reduce the number of mobile ions and limit ion mobility in the biopolymer electrolytes [45, 46].

The temperature dependence of ionic conductivity was investigated to determine the effects of temperature on the studied BPE. The study of the temperature dependence of conductivity was performed in the temperature range of 303–348 K. This measurement can be used to analyze the mechanism of ionic conduction of the biopolymer electrolytes. Figure 6 presents the temperature dependence with

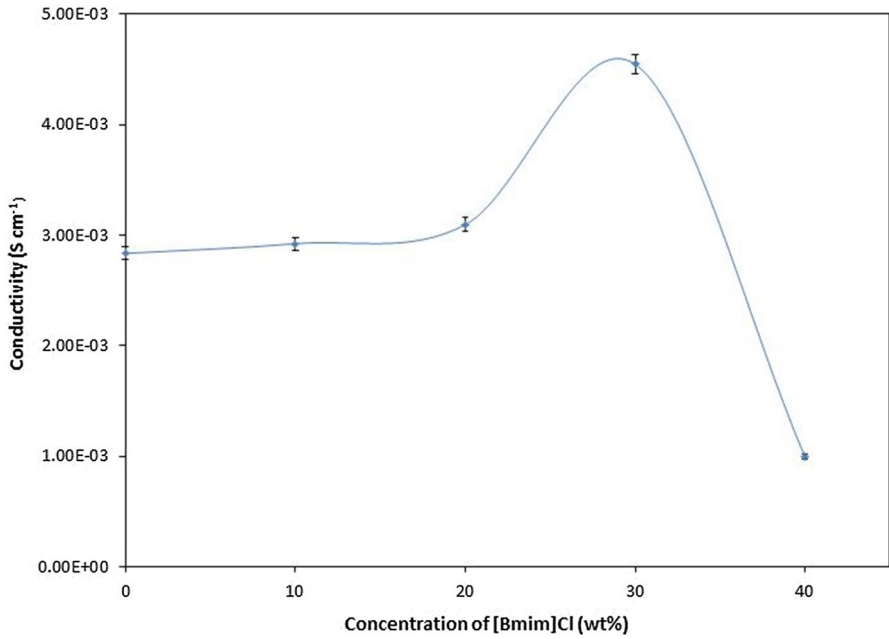


Fig. 5 Ionic conductivity of CMC-CH₃COONa-[Bmim]Cl at ambient temperature

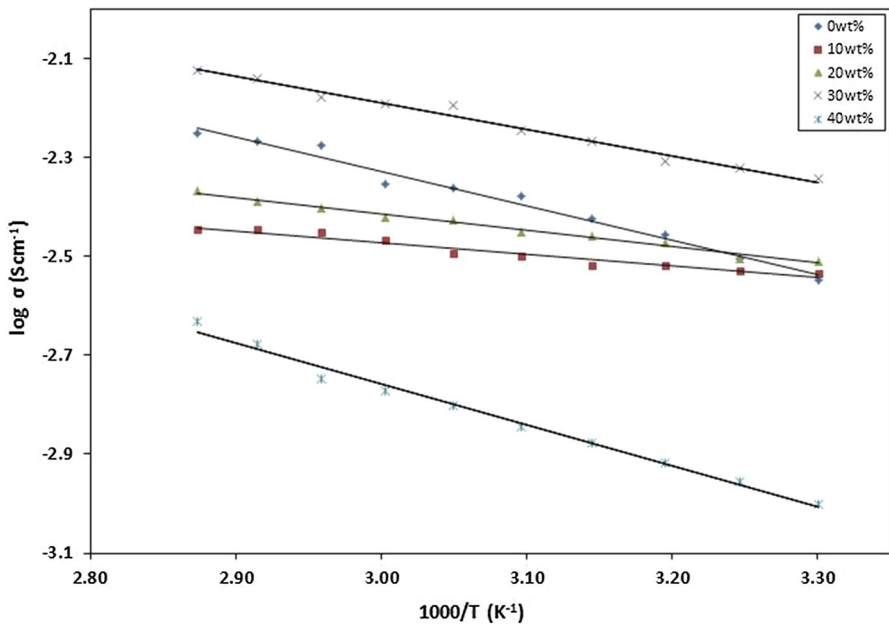


Fig. 6 Arrhenius plots of CMC-CH₃COONa containing 0–40 wt% of [Bmim]Cl

ionic conductivity for the biopolymer electrolyte films of different [Bmim]Cl compositions.

The linear variation of $\log \sigma$ versus $1000/T$ suggests Arrhenius behavior or thermally assisted behavior of ionic conductivity as expressed by:

$$\sigma = \sigma_0 \exp(-E_a/kT) \quad (2)$$

where σ_0 is the pre-exponential factor, E_a is the activation energy, k_b is the Boltzmann constant, and T is the absolute temperature. The regression values R^2 obtained from the linear fit of Arrhenius plots were close to unity ($R^2 \sim 1$). Conductivity did not show any abrupt change with temperature, indicating that no phase transition occurred in the polymer electrolytes at the selected temperature range. According to Aziz and co-workers [47], this relation indicates that conductivity is thermally assisted, which means that the variation in the temperature used affects the conductivity of samples. The nature of ion transport, Na^+ in this case, is quite similar to that occurring in ionic crystals; that is, the ions jump into the neighboring vacant sites [48, 49].

Activation energy, E_a , is the energy required to move an ion, presupposing that the structure remains unchanged, plus the energy required to deform the structure enough to allow the ion to pass. E_a was calculated from Eq. 2, and the results are depicted in Fig. 7.

Comparison of Figs. 5 and 7 indicates that E_a for conduction decreased gradually with the increase in conductivity, implying that the ions in the highly

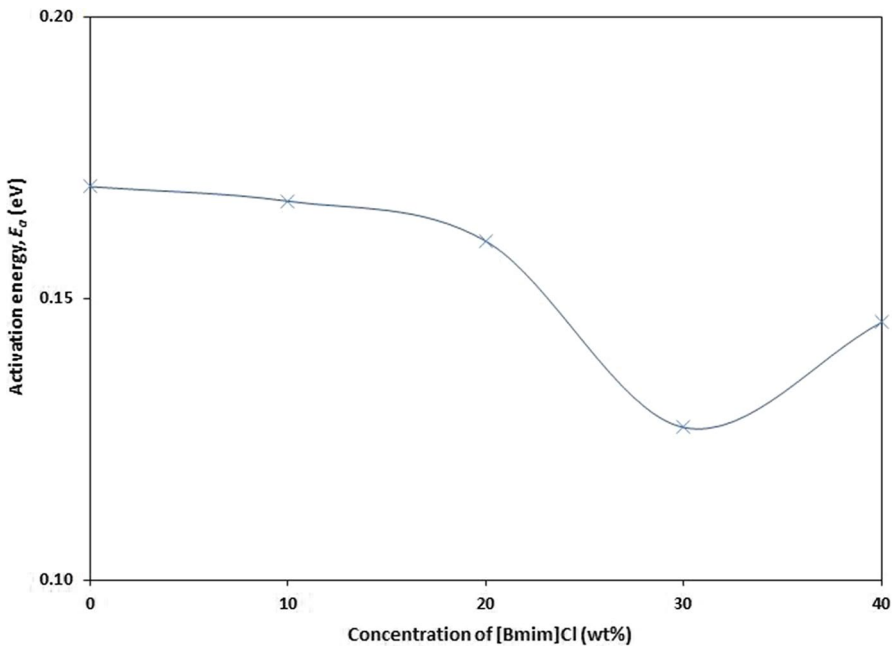


Fig. 7 Activation energy versus [Bmim]Cl concentration

conducting samples required low energy for migration. The samples with low E_a provided a small band gap, which allowed the conducting ions to be excited easily to a free ion-like state, thereby increasing the conductivity of the samples [50]. The E_a of CMC-CH₃COONa integrated with 30 wt% [Bmim]Cl was 0.13 eV. This E_a is considered low, suggesting that either Na⁺ or [Bmim]⁺ would break and rebind the coordination bond easily with a low energy barrier.

Dielectric relaxation study is a vital tool to elucidate the relaxation of dipoles in polymer electrolytes. In general, a polymer exhibits several kinds of dielectric absorption associated with various types of molecular relaxation. Moreover, dielectric relaxation study provides important insights into the polarization effect at the electrode/electrolyte interface, which can help in understanding conductivity trends [51]. According to Hema et al. [52], important insights into the ionic transport phenomenon can be obtained from the dielectric behavior of a system. In the current research, a dielectric study was performed to obtain insights into the ionic transport phenomenon of the CMC-CH₃COONa-Bmim[Cl] biosourced polymer electrolytes. The measured impedance data were used to calculate the real and imaginary parts of complex permittivity. Liedermann and Lapčík [53] stated that information on the motion of entities having an electric charge or an electric dipole moment can be obtained through dielectric analysis. Dielectric studies have examined two important parameters, namely dielectric constant, ϵ_r (known as storage component), and dielectric loss, ϵ_i (used to measure the energy loss for each cycle of the applied electric field) [52]. Both components can be calculated using the equations:

$$\epsilon_r(\omega) = \frac{Z_i}{\omega C_0(Z_r^2 + Z_i^2)} \tag{3}$$

$$\epsilon_i(\omega) = \frac{Z_r}{\omega C_0(Z_r^2 + Z_i^2)} \tag{4}$$

where $C_0 = \epsilon_0 A/t$, $\omega = 2\pi f$ (f is frequency), Z_r is the real part of impedance, Z_i is the imaginary part of impedance, A is the electrode–electrolyte contact area, and t is the thickness of the electrolyte.

Graphs of the dielectric constant and dielectric loss for the sample with the highest ionic conductivity of the CMC-CH₃COONa-Bmim[Cl] system are depicted in Figs. 8 and 9, respectively. The incorporation of ionic liquid Bmim[Cl], which acts as a plasticizer, into CMC-CH₃COONa complexes is expected to increase the degree of salt dissociation and enhance the number of free ions. Therefore, the increase in conductivity is due to the association of ions or decrease in mobility of the ions [54]. Figure 8 indicates the variation in ϵ_r and ϵ_i with angular frequency could be attributed to the formation of a space charge region at the electrode–electrolyte interface. This condition confirms non-Debye dependence and implies that the charge region with respect to frequency can be explained in terms of ion diffusion [50, 55]. No appreciable relaxation peaks were observed in the frequency range employed in this work.

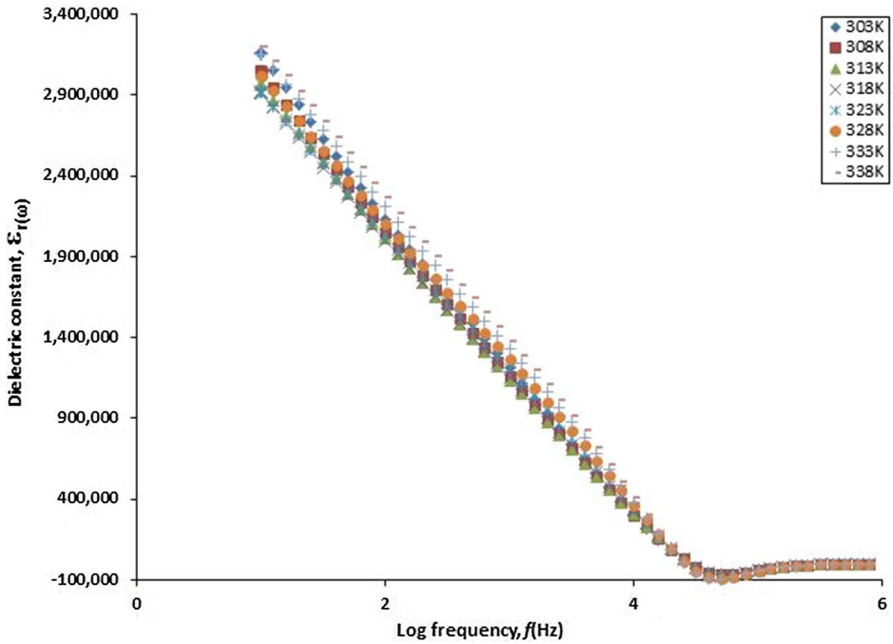


Fig. 8 Dielectric constant of CMC-CH₃COONa-30 wt% Bmim[Cl] biosourced polymer electrolyte recorded at different temperatures

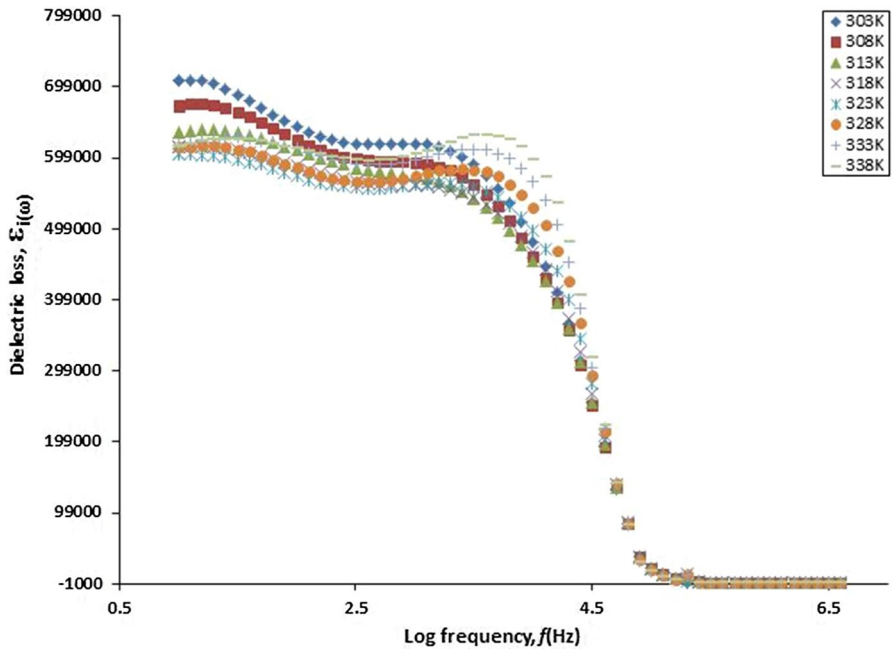


Fig. 9 Dielectric loss of CMC-CH₃COONa-30 wt% Bmim[Cl] biosourced polymer electrolytes

The dielectric plot in Fig. 8 illustrates a high value of dielectric constant ϵ_r in the low-frequency region. This phenomenon can be explained by the presence of blocking electrodes because the transfer of mobile ions in the external circuit could not be permitted, resulting in ion accumulation near the electrode and emergence of the bulk polarization effect in the materials [56]. Furthermore, the dipoles were unable to keep in pace with the fast-changing field due to the enhancement of frequency. This situation led to a drop in ϵ_r values with increasing frequency [57]. Meanwhile, dielectric loss ϵ_i increased at low frequencies, as depicted in Fig. 9, which can be explained by the free charge motion built up at the interface between the materials and electrodes. The ϵ_i trend showed the appearance of a dominant dielectric relaxation peak, whose maximum shifted gradually with the increment in frequency as the temperature increased. This high-frequency β -relaxation peak may have been by the side group dipoles [56].

Dielectric constant ϵ_r and dielectric loss ϵ_i increased with temperature, and this is due to the migration polarization of the mobile ions [58]. This phenomenon explains that heat or temperature increased the degree of salt dissociation and re-dissociation of ion aggregates, resulting in the enhancement of conductivity due to the increased content of free ions or charge carrier density. On the other hand, the value of ϵ_r and ϵ_i decreased with increasing frequency due to the high periodic reversal of the applied field. Therefore, the charge did not have enough time to build up at the interface. The polarization due to charge accumulation decreased, leading to a drop in the values of ϵ_r and ϵ_i [59, 60]. Further investigation of such dielectric behavior can be successfully achieved via a modulus study, which suppresses the effect of electrode polarization [61].

Transference number measurement

The normalized polarization current time plot for CMC-CH₃COONa containing 30 wt% [Bmim]Cl biopolymer electrolyte is shown in Fig. 10. The value of ionic transference number, t_{ion} , and electron transference number, t_e , may be derived using the equation:

$$t_{\text{ion}} = \frac{I_T - I_s}{I_T} \quad (5)$$

$$t_e = \frac{I_s}{I_T} \quad (6)$$

where I_i is the total initial current at start ($t=0$) (ionic and electronic) and I_s is the current on saturation (electronic current only); both are determined from the plot of normalized polarization current versus time.

The initial total current decreased with time due to the depletion of the ionic species in the biopolymer electrolytes and became constant in the fully depleted situation. Ionic migration occurred until the steady state was achieved. In the steady state, the cell was polarized, and any residual current flow was due to electron migration

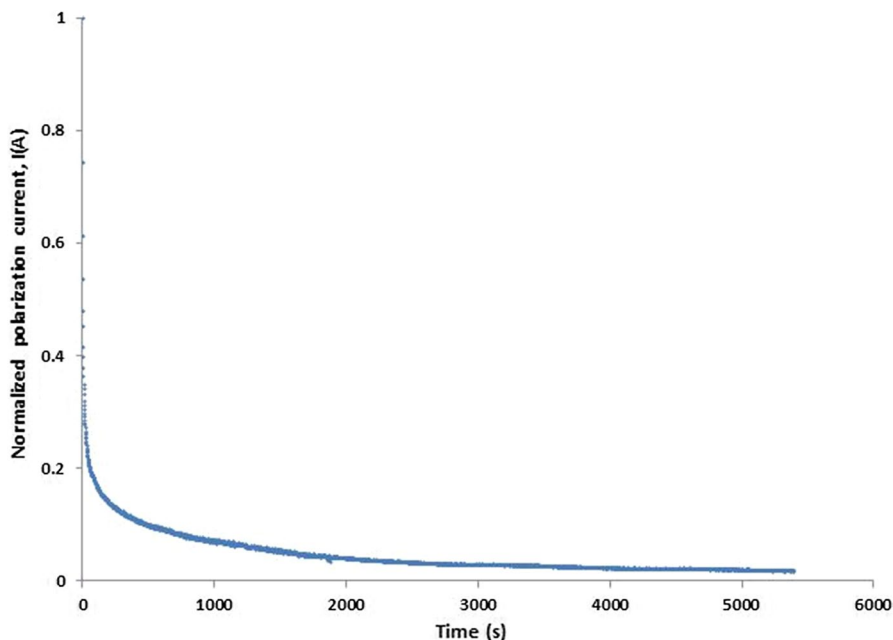


Fig. 10 Normalized polarization current versus time for the biopolymer electrolyte film of CMC-CH₃COONa-30 wt% [Bmim]Cl

across the electrolyte and interfaces. This phenomenon will occur if the biopolymer electrolyte is primarily ionic. The ionic currents through an ion-blocking electrode decrease rapidly with time [62, 63].

The t_i values for CMC-30 wt% CH₃COONa and CMC-CH₃COONa-30 wt% [Bmim]Cl electrolyte films are presented in Table 1. t_i for CMC-CH₃COONa was 0.99, showing that this system acted as an almost perfect ion conductor. This performance can be ascribed to the contribution of Na⁺ ions from CH₃COONa complexed with CMC. The result also suggests that the charge transports in the CMC-CH₃COONa system were predominantly due to ions with only a negligible electronic contribution [64].

The integration of [Bmim]Cl into the CMC-CH₃COONa BPE resulted in a reduction in t_i . Ramamohan and co-researchers [65] reported a similar reduction in t_i when a plasticizer was added to a (PEMA + PVC + NaIO₄) system. The decrease in t_i of the BPE was due to the increment in the number of ion pairs and neutral ion

Table 1 Biopolymer electrolytes transport numbers at ambient temperature

Biopolymer electrolyte film	Transport number		
	t_i	t_e	Total t
CMC-CH ₃ COONa	0.99	0.01	1.00
CMC-CH ₃ COONa-30 wt% [Bmim]Cl	0.95	0.05	1.00

aggregates that did not contribute any impact on ionic conduction. Meanwhile, a high t_i implies that most of the charge carriers in the BPE are ions.

The cationic transference number of the CMC electrolytes was determined with the Bruce and Vincent method as follows:

$$t_+ = \frac{I_{ss}}{I_0} \left[\frac{\Delta V - I_0 R_0}{\Delta V - I_{ss} R_{ss}} \right] \tag{7}$$

where I_0 is the initial current ($t=0$), R_0 is the electrolyte resistance before polarization, R_{ss} is the electrolyte resistance after polarization, I_{ss} is the steady-state current, and ΔV is the applied voltage pulse (1.0 V).

Figure 11 illustrates the chronoamperometry curve for the best conducting CMC-CH₃COONa-[Bmim]Cl. The calculated cationic transference number shows that CMC-CH₃COONa-[Bmim]Cl had a t_{Na^+} value of 0.129. The small value of cationic transference numbers might be due to oxygen in the polymer chains that trapped the cations electrostatically; ionic conduction was mostly contributed by anions [66, 67].

The addition of [Bmim]Cl (Bmim⁺ and Cl⁻) may decrease the fraction of Na⁺ to CH₃COO⁻ ions in the polymer. Na⁺ ions are surrounded by large number of Cl⁻ and CH₃COO⁻ anions forming an ionic cluster. The cationic transference number of electrolytes containing ionic liquid determined by Zygadlo-Monikowska et al.

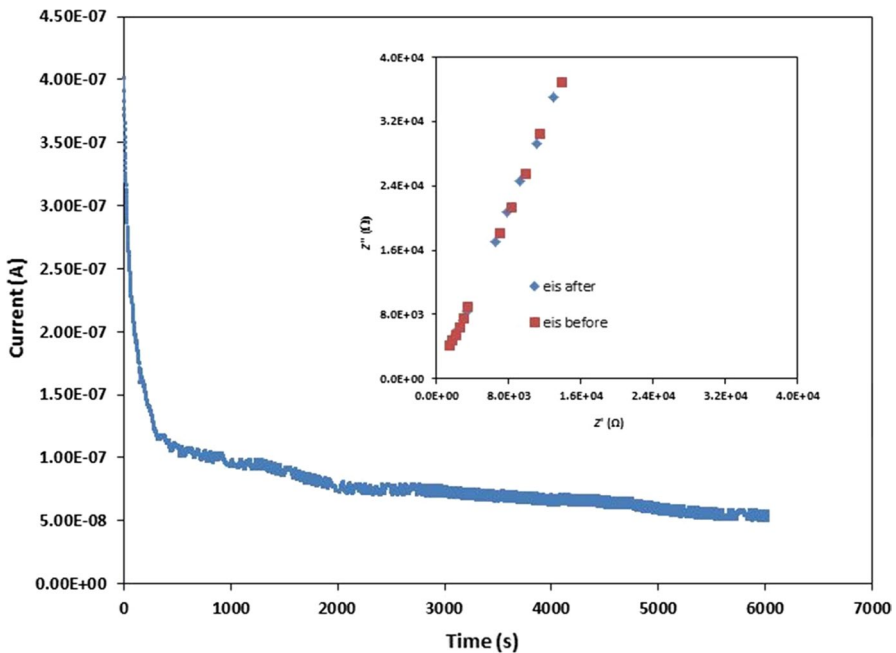


Fig. 11 Chronoamperometry curve for CMC-CH₃COONa-[Bmim]Cl electrolyte polarized with a potential 1.0 V. AC. The inset graph illustrates the impedance spectra of CMC-CH₃COONa-[Bmim]Cl electrolyte before and after polarization

[68] exhibited small cationic values in the range of 0.03–0.11. The work of Niedzicki et al. [69] also provided a low cationic transference number in the range of 0.02–0.04. The value obtained in this study is comparable with those reported in literature. Therefore, this result indicates that the majority of ions that contribute to ionic conductivity are not cations (Bmim^+ or Na^+), but most possibly anions (Cl^- or CH_3COO^- [70, 71]).

Electrochemical stability

An electrochemical stability study was conducted on the CMC- CH_3COONa system incorporated with 30 wt% $[\text{Bmim}]\text{Cl}$ because it is the best conducting BPE. Figure 12 presents a voltammogram of CMC- CH_3COONa -30 wt% of $[\text{Bmim}]\text{Cl}$. The graph shows that the BPE was stable until 2.9 V and it is expected to be the BPE breakdown voltage. This result reveals that the electrolyte is ideal for the fabrication of Na batteries.

Fabrication and performance of sodium batteries

The main components in a battery are the anode, cathode and electrolyte. Oxidation occurs in the anode (negative terminal of the battery in the discharged mode), from where electrons flow to the external circuit. Reduction occurs in the cathode (positive terminal of the battery in the discharged mode), to which the electrons flow into the external circuit. The anode must be an effective oxidizing agent, be stable in adhesion with the electrolyte and have a suitable working voltage and long life time. The cathode must have several characteristics such as being a good reducing agent and easy to fabricate, having good conductivity and low cost. Electrolyte is the intermediate through which ions are transported between the anode and cathode during charge and discharge in electrochemical devices [72]. Usually electrolytes with conductivity range between 10^{-5} and 10^{-2} S cm^{-1} and an ionic transference number is greater than 0.9; hence, they are suitable for battery applications [58].

The CMC- CH_3COONa -30 wt% $[\text{Bmim}]\text{Cl}$ system exhibits the highest conductivity. Therefore, this system was used as the electrolyte to fabricate Na batteries in

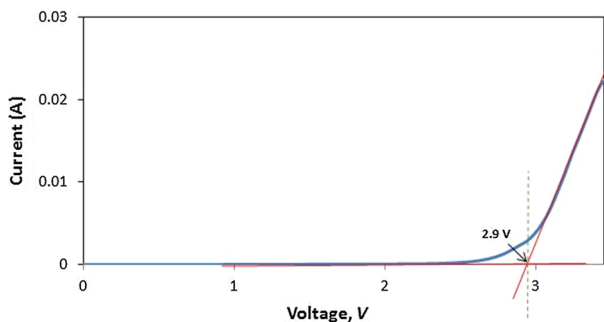


Fig. 12 LSV curve of CMC- CH_3COONa -30 wt% $[\text{Bmim}]\text{Cl}$

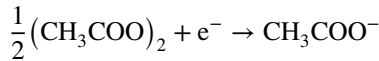
this study. Solid-state Na batteries were fabricated with a configuration of Na/CMC-CH₃COONa-30 wt% [Bmim]Cl/I₂+C+electrolyte. Figure 13 displays the schematic architecture of the fabricated Na battery (coin cell).

From the configuration, the half-cell reactions can be written as follows.

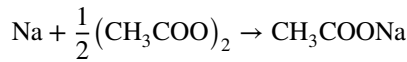
At the anode:



At the cathode:



The overall reaction can be written as:



The open circuit voltage (OCV) of the constructed Na battery was monitored for 24 h and plotted against time, as shown in Fig. 14. OCV is the difference in electric potential between two terminals of a device when it is disconnected from any circuit. No external electric current flow existed between the two terminals. OCV is determined to obtain the maximum voltage and stability of the battery, and the determination process was conducted for 24 h. The OCV of the cell at ambient temperature showed an initial voltage of 1.68 V, which decreased to 1.6 V in the first 6 h of assembly. This phenomenon could be due to the oxidation of the anode [73]. The discharged capacity and other parameters of the fabricated battery were calculated with the following formula:

$$\text{Power density} = \frac{\text{Current} \times \text{Voltage (in plateau region)}}{\text{Weight of cell}} \tag{8}$$

$$\text{Energy density} = \text{Power density} \times \text{Discharged time (in plateau region)} \tag{9}$$

$$\text{Internal resistance} = \frac{\text{Open circuit voltage} - \text{voltage}}{\text{Current}} \tag{10}$$

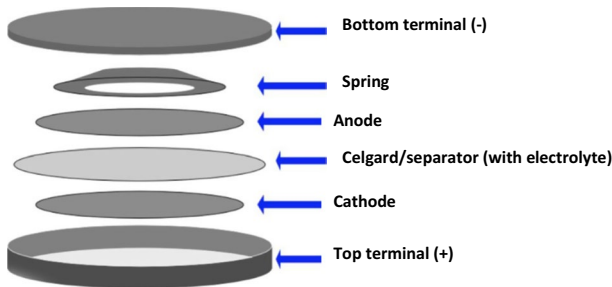


Fig. 13 Schematic architecture for the fabrication of coin cell

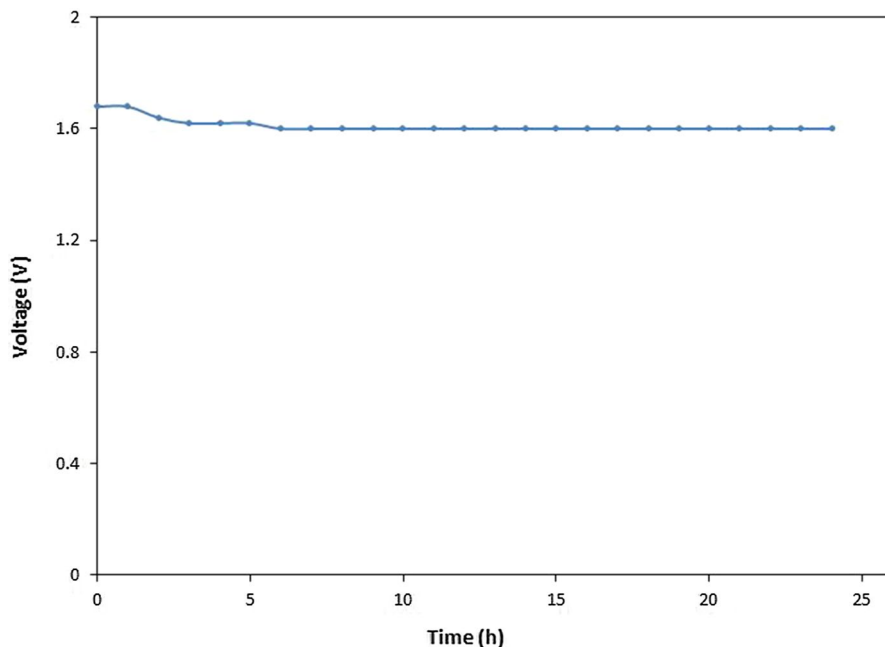


Fig. 14 OCV as a function of time for CMC-CH₃COONa-30 wt% [Bmim]Cl

$$\text{Discharged capacity} = \text{Current} \times \text{Discharged time (in plateau region)} \quad (11)$$

The discharge profile of the constructed NIB is shown in Fig. 15. The battery was discharged at a constant current of 0.1 mA. The load voltage of the battery decreased to 1.13 V from 1.54 V within 50 h after assembly. The initial sharp decrease in cell voltage was attributed to the polarization effect and/or formation of a thin layer of Na salt at the electrode–electrolyte interface [74]. The OCV and discharge time for the plateau region and the other cell parameters for this cell are listed in Table 2. The battery application indicates that this battery is suitable for low-current–density application. However, further work needs to be done to improve the characteristics of polymer electrolytes and obtain electrochemical cells with ideal performance.

Conclusions

The effects of [Bmim]Cl on the biopolymer electrolytes of kenaf fiber-based CMC impregnated with CH₃COONa were successfully explored. FTIR analysis confirmed the interaction between the polymer host with Na salt and the ionic liquid. SEM revealed an enhancement in the amorphous region after introducing the ionic liquid into the biopolymer system. [Bmim]Cl influenced the ionic conductivity of the biopolymer electrolytes, and the best value of $(4.54 \pm 1.2) \times 10^{-3} \text{ S cm}^{-1}$ was obtained for the system containing 30 wt% of [Bmim]Cl. LSV result showed that electrochemical stability reached $\sim 2.9 \text{ V}$, showing that the biopolymer electrolyte

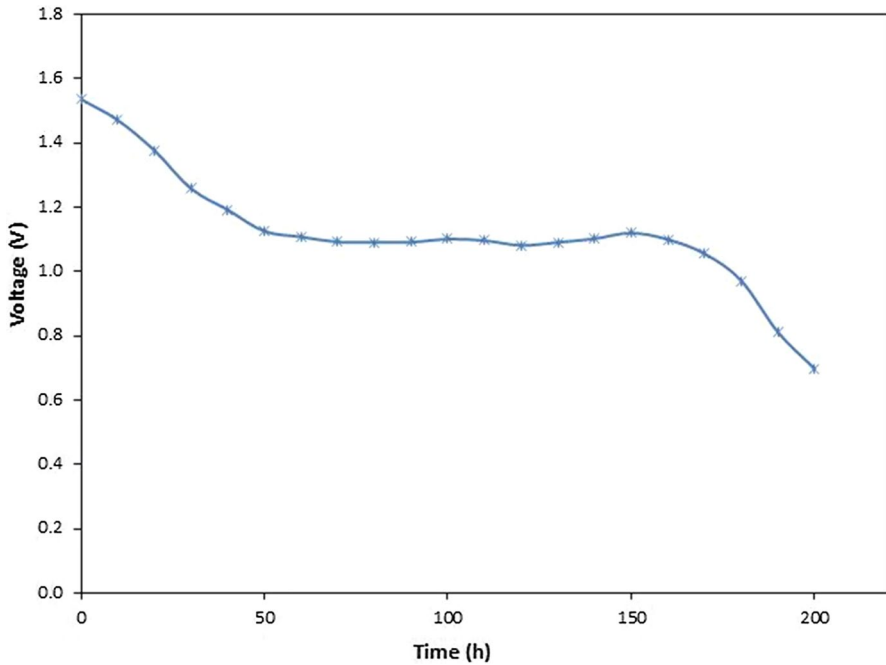


Fig. 15 Discharged characteristic of CMC-CH₃COONa-30 wt% [Bmim]Cl

Table 2 Cell parameters of Na/CMC-CH₃COONa-30 wt% [Bmim]Cl/I₂ + C + electrolyte

Cell parameters	Measured values of discharged 0.1 mA
Cell area (cm ²)	1.33
Cell weight (g)	0.75
Effective cell diameter (cm)	1.3
Cell thickness (cm)	0.1
Open circuit voltage (V)	1.6
Discharged time for plateau region (h)	150
Current density (μA cm ⁻²)	32.7
Discharged capacity (mAh)	1.5
Power density (mW kg ⁻¹)	14.65
Energy density (Wh kg ⁻¹)	2197.5

is suitable for practical application in electrochemical devices. The electrochemical cell was applied with the optimized BPE film, which successfully acted as the electrolyte and separator in the electrochemical cell.

Acknowledgements The work was financially supported by MI-2019-018 and DIP-2015-028 (Dana Impak Perdana) from Centre of Research and Instrument Management, Universiti Kebangsaan Malaysia.

References

1. Yoldaş Y, Önen A, Muyeen S, Vasilakos AV, Alan İ (2017) Enhancing smart grid with micro-grids: challenges and opportunities. *Renew Sustain Energy Rev* 72:205–214
2. Carrasco JM, García Franquelo L, Bialasiewicz JT, Galván E, Portillo Guisado RC, MdlÁ Martín Prats, León JI, Moreno-Alfonso N (2006) Power-electronic systems for the grid integration of renewable energy sources: a survey. *IEEE Trans Ind Electron* 53(4):1002–1016
3. Shafiullah G, Oo AM, Ali AS, Wolfs P (2013) Potential challenges of integrating large-scale wind energy into the power grid—a review. *Renew Sustain Energy Rev* 20:306–321
4. Su'ait MS, Rahman MYA, Ahmad A (2015) Review on polymer electrolyte in dye-sensitized solar cells (DSSCs). *Sol Energy* 115:452–470
5. Pan H, Hu YS, Chen L (2013) Room-temperature stationary sodium-ion batteries for large-scale electric energy storage. *Energy Environ Sci* 6(8):2338–2360
6. MacFarlane DR, Tachikawa N, Forsyth M, Pringle JM, Howlett PC, Elliott GD, Davis JH, Watanabe M, Simon P, Angell CA (2014) Energy applications of ionic liquids. *Energy Environ Sci* 7(1):232–250
7. Zhu YH, Yang X, Bao D, Bie XF, Sun T, Wang S, Jiang Y-S, Zhang XB, Yan JM, Jiang Q (2018) High-energy-density flexible potassium-ion battery based on patterned electrodes. *Joule* 2(4):736–746
8. Demir-Cakan R, Palacin MR, Croguennec L (2019) Rechargeable aqueous electrolyte batteries: from univalent to multivalent cation chemistry. *J Mater Chem A* 7(36):20519–20539
9. Noor SAM, Ahmad A, Talib I, Rahman MYA (2010) Morphology, chemical interaction, and conductivity of a PEO-ENR50 based on solid polymer electrolyte. *Ionics* 16(2):161–170
10. Imperiyka M, Ahmad A, Hanifah SA, Rahman MYA (2013) Potential of UV-curable poly (glycidyl methacrylate-co-ethyl methacrylate)-based solid polymer electrolyte for lithium ion battery application. *Int J Electrochem Sci* 8(9):10932–10945
11. Mohtadi R, Mizuno F (2014) Magnesium batteries: current state of the art, issues and future perspectives. *Beilstein J Nanotechnol* 5(1):1291–1311
12. Noor SAM, Howlett PC, MacFarlane DR, Forsyth M (2013) Properties of sodium-based ionic liquid electrolytes for sodium secondary battery applications. *Electrochim Acta* 114:766–771
13. Gao T, Wang B, Wang L, Liu G, Wang F, Luo H, Wang D (2018) LiAlCl₄·3SO₂ as a high conductive, non-flammable and inorganic non-aqueous liquid electrolyte for lithium ion batteries. *Electrochim Acta* 286:77–85
14. Colò F, Bella F, Nair JR, Gerbaldi C (2017) Light-cured polymer electrolytes for safe, low-cost and sustainable sodium-ion batteries. *J Power Sour* 365:293–302
15. Kim SW, Seo DH, Ma X, Ceder G, Kang K (2012) Electrode materials for rechargeable sodium-ion batteries: potential alternatives to current lithium-ion batteries. *Adv Energy Mater* 2(7):710–721
16. Yamauchi H, Ikejiri J, Tsunoda K, Tanaka A, Sato F, Honma T, Komatsu T (2020) Enhanced rate capabilities in a glass-ceramic-derived sodium all-solid-state battery. *Sci Rep* 10(1):1–12
17. Yabuuchi N, Kubota K, Dahbi M, Komaba S (2014) Research development on sodium-ion batteries. *Chem Rev* 114(23):11636–11682
18. Bella F, Muñoz-García AB, Colò F, Meligrana G, Lamberti A, Destro M, Pavone M, Gerbaldi C (2018) Combined structural, chemometric, and electrochemical investigation of vertically aligned TiO₂ nanotubes for Na-ion batteries. *ACS Omega* 3(7):8440–8450
19. Guan B, Qi SY, Li Y, Sun T, Liu YG, Yi TF (2020) Towards high-performance anodes: design and construction of cobalt-based sulfide materials for sodium-ion batteries. *J Energy Chem* 54:680–698
20. Piana G, Ricciardi M, Bella F, Cucciniello R, Proto A, Gerbaldi C (2020) Poly (glycidyl ether) s recycling from industrial waste and feasibility study of reuse as electrolytes in sodium-based batteries. *Chem Eng J* 382:122934
21. Chen G, Zhang K, Liu Y, Ye L, Gao Y, Lin W, Xu H, Wang X, Bai Y, Wu C (2020) Flame-retardant gel polymer electrolyte and interface for quasi-solid-state sodium ion batteries. *Chem Eng J* 401:126065
22. Rani MSA, Rudhziah S, Ahmad A, Mohamed NS (2014) Biopolymer electrolyte based on derivatives of cellulose from kenaf bast fiber. *Polymers* 6(9):2371–2385
23. Arof AK, Amirudin S, Yusof SZ, Noor IM (2014) A method based on impedance spectroscopy to determine transport properties of polymer electrolytes. *Phys Chem Chem Phys* 16(5):1856–1867

24. Wagner JB, Wagner C (1957) Electrical conductivity measurements on cuprous halides. *J Chem Phys* 26(6):1597–1601
25. Thangadurai V, Weppner W (2002) Determination of the sodium ion transference number of the Dion–Jacobson-type layered perovskite $\text{NaCa}_2\text{Nb}_3\text{O}_{10}$ using ac impedance and dc methods. *Chem Mater* 14(3):1136–1143
26. Zhou Y, Fu S, Zhang L, Zhan H (2013) Superabsorbent nanocomposite hydrogels made of carboxylated cellulose nanofibrils and CMC-gp (AA-co-AM). *Carbohydr Polym* 97(2):429–435
27. Rani MSA, Hassan NH, Ahmad A, Kaddami H, Mohamed NS (2016) Investigation of biosourced carboxymethyl cellulose-ionic liquid polymer electrolytes for potential application in electrochemical devices. *Ionics* 22(10):1855–1864
28. Lii CY, Tomasik P, Zaleska H, Liaw SC, Lai VMF (2002) Carboxymethyl cellulose–gelatin complexes. *Carbohydr Polym* 50(1):19–26
29. Taleb MFA, El-Mohdy HA, El-Rehim HA (2009) Radiation preparation of PVA/CMC copolymers and their application in removal of dyes. *J Hazard Mater* 168(1):68–75
30. Donova I, Stefov V, Aleksovska S (2001) Synthesis, characterization and thermal decomposition of hydroxylammonium uranyl acetate. *J Therm Anal Calorim* 63(1):125–132
31. Shamsudin IJ, Ahmad A, Hassan NH, Kaddami H (2015) Biopolymer electrolytes based on carboxymethyl κ -carrageenan and imidazolium ionic liquid. *Ionics* 22(6):841–851
32. Ramesh S, Liew C-W, Morris E, Durairaj R (2010) Effect of PVC on ionic conductivity, crystallographic structural, morphological and thermal characterizations in PMMA–PVC blend-based polymer electrolytes. *Thermochim Acta* 511(1):140–146
33. Lam E, Leung AC, Liu Y, Majid E, Hrapovic S, Male KB, Luong JH (2012) Green strategy guided by Raman spectroscopy for the synthesis of ammonium carboxylated nanocrystalline cellulose and the recovery of byproducts. *ACS Sustain Chem Eng* 1(2):278–283
34. Stephan AM, Saito Y, Muniyandi N, Renganathan N, Kalyanasundaram S, Elizabeth RN (2002) Preparation and characterization of PVC/PMMA blend polymer electrolytes complexed with $\text{LiN}(\text{CF}_3\text{SO}_2)_2$. *Solid State Ionics* 148(3):467–473
35. Baranyai KJ, Deacon GB, MacFarlane DR, Pringle JM, Scott JL (2004) Thermal degradation of ionic liquids at elevated temperatures. *Aust J Chem* 57(2):145–147
36. Biswal DR, Singh RP (2004) Characterisation of carboxymethyl cellulose and polyacrylamide graft copolymer. *Carbohydr Polym* 57(4):379–387
37. Shukur MF, Ithnin R, Kadir MFZ (2014) Electrical properties of proton conducting solid biopolymer electrolytes based on starch–chitosan blend. *Ionics* 20(7):977–999
38. Ramya CS, Selvasekarapandian S, Savitha T, Hirankumar G, Angelo PC (2007) Vibrational and impedance spectroscopic study on PVP– NH_4SCN based polymer electrolytes. *Physica B Condens Matter* 393(1):11–17
39. Jacob MME, Prabakaran SRS, Radhakrishna S (1997) Effect of PEO addition on the electrolytic and thermal properties of PVDF– LiClO_4 polymer electrolytes. *Solid State Ionics* 104(3):267–276
40. Jurado JF, Trujillo JA, Mellander BE, Vargas RA (2003) Effect of AgBr on the electrical conductivity of β -AgI. *Solid State Ionics* 156(1):103–112
41. Lee TK, Zaini NFM, Mobarak NN, Hassan NH, Noor SAM, Mamat S, Loh KS, KuBulat KH, Su'ait MS, Ahmad A (2019) PEO based polymer electrolyte comprised of epoxidized natural rubber material (ENR50) for Li-Ion polymer battery application. *Electrochim Acta* 316:283–291
42. Anuar NK, Subban RHY, Mohamed NS (2012) Properties of PEMA– $\text{NH}_4\text{CF}_3\text{SO}_3$ added to BMATSF1 ionic liquid. *Materials* 5(12):2609–2620
43. Shamsudin IJ, Ahmad A, Hassan NH, Kaddami H (2015) Bifunctional ionic liquid in conductive biopolymer based on chitosan for electrochemical devices application. *Solid State Ionics* 278:11–19
44. Woo HJ, Majid SR, Arof AK (2011) Conduction and thermal properties of a proton conducting polymer electrolyte based on poly (ϵ -caprolactone). *Solid State Ionics* 199:14–20
45. Radzir NNM, Hanifah SA, Ahmad A, Hassan NH, Bella F (2015) Effect of lithium bis (trifluoromethylsulfonyl) imide salt-doped UV-cured glycidyl methacrylate. *J Solid State Electrochem* 19(10):3079–3085
46. Su'ait MS, Ahmad A, Hamzah H, Rahman MYA (2011) Effect of lithium salt concentrations on blended 49% poly (methyl methacrylate) grafted natural rubber and poly (methyl methacrylate) based solid polymer electrolyte. *Electrochim Acta* 57:123–131
47. Aziz NN, Idris NK, Isa MIN (2010) Proton conducting polymer electrolytes of methylcellulose doped ammonium fluoride: conductivity and ionic transport studies. *J Phys. Sci* 5(6):748–752

48. Ramesh S, Yahaya AH, Arof AK (2002) Dielectric behaviour of PVC-based polymer electrolytes. *Solid State Ionics* 152:291–294
49. Souquet JL, Levy M, Duclot M (1994) A single microscopic approach for ionic transport in glassy and polymer electrolytes. *Solid State Ionics* 70:337–345
50. Khiar AA, Arof AK (2010) Conductivity studies of starch-based polymer electrolytes. *Ionics* 16(2):123–129
51. Howell FS, Bose RA, Macedo PB, Moynihan CT (1974) Electrical relaxation in a glass-forming molten salt. *J Phys Chem* 78(6):639–648
52. Hema M, Selvasekerapandian S, Sakunthala A, Arunkumar D, Nithya H (2008) Structural, vibrational and electrical characterization of PVA–NH₄Br polymer electrolyte system. *Physica B Condens Matter* 403(17):2740–2747
53. Liedermann K, Lapčik L (2000) Dielectric relaxation in hydroxyethyl cellulose. *Carbohydr Polym* 42(4):369–374
54. Rajendran S, Sivakumar M, Subadevi R (2004) Investigations on the effect of various plasticizers in PVA–PMMA solid polymer blend electrolytes. *Mater Lett* 58(5):641–649
55. Macdonald JR (1987) Impedance spectroscopy, vol 11. Wiley, New York
56. Tamilselvi P, Hema M (2014) Conductivity studies of LiCF₃SO₃ doped PVA: PVdF blend polymer electrolyte. *Physica B Condens Matter* 437:53–57
57. Devi PI, Ramachandran K (2011) Dielectric studies on hybridised PVDF–ZnO nanocomposites. *J Exp Nanosci* 6(3):281–293
58. MacCallum J, Vincent C (1987) Ion-molecule and ion-ion interactions. *Polym Electrolyte Rev* 1:23–37
59. Hamsan MH, Shukur MF, Kadir MFZ (2017) NH₄NO₃ as charge carrier contributor in glycerolized potato starch-methyl cellulose blend-based polymer electrolyte and the application in electrochemical double-layer capacitor. *Ionics* 23(12):3429–3453
60. Tripathi M, Tripathi SK (2017) Electrical studies on ionic liquid-based gel polymer electrolyte for its application in EDLCs. *Ionics* 23(10):2735–2746
61. Shastry MCR, Rao KJ (1991) Ac conductivity and dielectric relaxation studies in AgI-based fast ion conducting glasses. *Solid State Ionics* 44(3–4):187–198
62. Rani MSA, Ahmad A, Mohamed NS (2018) A comprehensive investigation on electrical characterization and ionic transport properties of cellulose derivative from kenaf fibre-based biopolymer electrolytes. *Polym Bull* 75(11):5061–5074
63. Ibrahim S, Ahmad A, Mohamed NS (2018) Comprehensive studies on polymer electrolyte and dye-sensitized solar cell developed using castor oil-based polyurethane. *J Solid State Electrochem* 22(2):461–470
64. Linford R (1988) Experimental techniques for studying polymer electrolytes. *Solid state ionics devices*. World Scientific, Singapore, pp 551–571
65. Ramamohan K, Sharma AK (2013) Effect of plasticizer on (PVC + PEMA + NaIO₄) solid polymer blend electrolyte system for battery characterization studies. *Adv Polym Sci Technol* 3:49–53
66. Sequeira C, Santos D (2010) Polymer electrolytes: fundamentals and applications. Elsevier, Amsterdam
67. Dzulkurnain NA, Rani MSA, Ahmad A, Mohamed NS (2018) Effect of lithium salt on physico-chemical properties of P (MMA-co-EMA) based copolymer electrolytes for dye-sensitized solar cell application. *Ionics* 24(1):269–276
68. Zygadło-Monikowska E, Florjańczyk Z, Kubisa P, Biedroń T, Sadurski W, Puczyłowska A, Langwald N, Ostrowska J (2014) Lithium electrolytes based on modified imidazolium ionic liquids. *Int J Hydrog Energy* 39(6):2943–2952
69. Niedzicki L, Karpierz E, Bitner A, Kasprzyk M, Zukowska GZ, Marcinek M, Wieczorek W (2014) Optimization of the lithium-ion cell electrolyte composition through the use of the LiTDI salt. *Electrochim Acta* 117:224–229
70. Bhargav PB, Mohan VM, Sharma A, Rao VN (2009) Investigations on electrical properties of (PVA: NaF) polymer electrolytes for electrochemical cell applications. *Curr Appl Phys* 9(1):165–171
71. Ali AMM, Yahya MZA, Bahron H, Subban RHY (2006) Electrochemical studies on polymer electrolytes based on poly (methyl methacrylate)-grafted natural rubber for lithium polymer battery. *Ionics* 12(4–5):303–307
72. Stephan AM, Nahm K (2006) Review on composite polymer electrolytes for lithium batteries. *Polymer* 47(16):5952–5964

73. Samsudin AS, Lai HM, Isa MIN (2014) Biopolymer materials based carboxymethyl cellulose as a proton conducting biopolymer electrolyte for application in rechargeable proton battery. *Electrochim Acta* 129:1–13
74. Reddy RN, Reddy RG (2003) Sol–gel MnO₂ as an electrode material for electrochemical capacitors. *J Power Sour* 124(1):330–337

Publisher's Note Springer Nature remains neutral with regard to jurisdictional claims in published maps and institutional affiliations.

Affiliations

Mohd Saiful Asmal Rani^{1,3}  · **Masita Mohammad¹** · **Mohd Sukor Sua'it¹** · **Azizan Ahmad²** · **Nor Sabirin Mohamed³**

Mohd Sukor Sua'it
mohdsukor@ukm.edu.my

Azizan Ahmad
azizan@ukm.edu.my

Nor Sabirin Mohamed
nsabirin@um.edu.my

- ¹ Solar Energy Research Institute (SERI), Universiti Kebangsaan Malaysia, 43600 Bangi, Selangor, Malaysia
- ² School of Chemical Sciences, Faculty of Science and Technology, Universiti Kebangsaan Malaysia, 43600 Bangi, Selangor, Malaysia
- ³ Centre for Foundation Studies in Science, University of Malaya, 50603 Kuala Lumpur, Malaysia